Condensed Matter Physics, 2024, Vol. 27, No. 2, 23201: 1–17
DOI: 10.5488/CMP.27.23201
http://www.icmp.lviv.ua/journal

CONDENSED MATTER PHYSICS

Molecular dynamics simulations of water-ethanol mixtures. I. Composition trends in thermodynamic properties

D. Benavides Bautista[1], M. Aguilar [2], O. Pizio [2] *

[1] Instituto de Ciencias Básicas y Ingeniería, Universidad Autónoma de Estado de Hidalgo, Pachuca de Soto, Hidalgo 42039, México

[2] Instituto de de Química, Universidad Nacional Autónoma de México, Circuito Exterior, 04510, Cd. Mx., México

Received April 16, 2024, in final form May 20, 2024

We explored the composition dependence of a rather comprehensive set of properties of liquid water-ethanol mixtures by using the isobaric-isothermal molecular dynamics computer simulations. The united atom non-polarizable model from the TraPPE data basis for the ethanol molecule combined with the TIP4P-2005 and SPC/E water models is considered. We restrict our calculations to atmospheric pressure, 0.1013 MPa, and room temperature, 298.15 K. Composition trends of the behavior of density, excess mixing volume, apparent molar volumes are described. On the other hand, the excess mixing enthalpy and partial molar enthalpies of species are reported. Besides, we explore the coefficient of isobaric thermal expansion, isothermal heat capacity, adiabatic bulk modulus and heat capacity at constant pressure. In addition, the self-diffusion coefficients of species, the static dielectric constant and the surface tension are described. We intend to get insights into peculiarities of mixing of species in the mixture upon changes of ethanol molar fraction. The quality of predictions of the models is critically evaluated by detailed comparisons with experimental results. Then, necessary improvements of the modelling are discussed.

Key words: *molecular dynamics, water-ethanol mixtures, surface tension, dielectric constant, partial molar volumes*

1. Introduction

One of us (O.P.) with profound sadness would like to dedicate this work to the memory of his former scientific supervisor and founder of the Condensed Matter Physics journal, Prof. Ihor Yukhnovskyi, who passed away recently.

This manuscript presents the results of the first part of our project focused on the properties of water-ethanol mixtures. It refers to the description of the composition dependence of thermodynamic and other related issues of mixing of water and ethanol species at room temperature and at ambient pressure. To do that we use molecular dynamics computer simulations. All aspects of the evolution of the microscopic structure and of hydrogen bonds network will be discussed in future, in our subsequent report.

Liquid mixtures of water and ethanol are of much practical importance as solvents and reaction media in organic chemistry, medicinal and food chemistry, and in chemical engineering. Pure ethanol and its mixtures with water have been investigated by several experimental techniques since the times of Mendeleev. The experimental knowledge and understanding of the microscopic structure and dynamic properties of the systems in question mainly follow from the application of neutron scattering, nuclear magnetic resonance, dielectric relaxation, vibrational and Raman spectroscopy methods [1–4]. On the other hand, calorimetric studies yield a valuable set of thermodynamic data for the mixtures in question [5–

*Corresponding author: oapizio@gmail.com.

9]. Dynamic light scattering studies contributed to the elucidation of anomalous behaviors in water-ethanol mixtures as well, see, e.g., [10] and references in [11, 12].

In order to interpret the experimental observations in every detail and to get ampler insights, one is usually forced to resort to computer simulation methodology. A common strategy of computer simulations methodology is to choose a model of each species, water and ethanol in the present case, and assume the cross interactions by using the combination rules. Then, software based on strict rules of statistical mechanics is applied. Appropriateness of the computer simulations predictions for a given model for a mixture, upon changing temperature, T, pressure, P, and composition, X, variables, is then tested by comparison with reference experimental data.

Profound insights into the properties of pure components of interest of the present study from computer simulations are available. Namely, a comprehensive set of data for non-polarizable water models were provided by Vega and Abascal [13]. A similar type of strategy of description was applied to methanol [14]. In the case of ethanol and higher alcohols, the situation is less satisfactory. We are not aware of the work describing an ample set of ethanol properties using different models with their critical evaluation versus experimental data. Certain aspects of the microscopic structure and some properties of pure ethanol were studied in [15–17]. On the other hand, many computer simulation studies were performed for water-ethanol mixtures. They differ in the modelling of water component. Specifically, the TIP3P water model was used in [18]. Wensink et al.[19] used the TIP4P water model. However, most frequently well tested SPC/E [20] and TIP4P-2005 [21] models were used to describe water species [22–27]. Concerning ethanol species, various models were involved. All of them have roots in the OPLS developments of Jorgensen et al. [28, 29]. Namely, the works from the Croatian laboratory explored versions of the united atom model for ethanol [23] (the CH_3 and CH_2 groups are considered as sites) including the TraPPE version [30]. The works from the Hungarian laboratory of L. Pusztai focused on the OPLS all atom models [25]. Similar modelling was used by Wensink et al. [19]. The united atom type models were used in [31, 32]. Finally, the attempt to study water-ethanol mixture using polarizable models for two components was undertaken as well [33]. The united site models are computationally less time-consuming, in comparison with more sophisticated ones. They can be used, however, with a certain degree of confidence, to elucidate the mixing trends of species and to describe thermodynamic properties. On the other hand, these models have some disadvantages; since not all the atoms are represented, they miss some of the partial radial distribution functions and stereochemical information, such as some bond angles and dihedral angles. Therefore, if one focuses on the microscopic structure in terms of the total structure factor to compare with experimental results, it is appropriate to perform simulations with all-atom models, see, e.g., [25, 34].

Having this discussion in mind, the principal objective of the present work is to obtain a rather comprehensive set of results for the composition dependence of water-ethanol mixtures at atmospheric pressure and at room temperature by using isobaric-isothermal molecular dynamics computer simulation. The reason is that several previous publications were focused on the interval of low ethanol concentration. Namely, elucidation of anomalies of composition behavior, or better say of non-monotonous behaviors of different properties and their interpretation from molecular dynamics simulations, is explored. Moreover, a restricted set of properties of the systems in question is usually considered. Consequently, the validation of the models used in computer simulations is not complete.

2. Models and simulation details

In this work we restrict our attention to a single united atom type, non-polarizable model with four sites, O, H, CH_2, CH_3 for ethanol [30]. Within this type of modelling, the interaction potential between all atoms and/or groups is assumed as a sum of Lennard-Jones (LJ) and Coulomb terms. The parameters are given in the web page of the TraPPE data basis (http://trappe.oit.umn.edu) and in the original publication [30]. For water, the TIP4P-2005 [21] and SPC/E [20] models are used. Lorentz-Berthelot combination rules were used to determine the cross parameters for the relevant potential well depths and diameters.

Molecular dynamics computer simulations of water-ethanol mixtures are performed in the isothermal - isobaric (NPT) ensemble at atmospheric pressure 1 bar and at temperature 298.15 K. We used GROMACS

package [35] version 5.1.2. The simulation box in each run was cubic, the total number of molecules of both species is fixed at 3000. Composition of the mixture is described by the molar fraction of ethanol molecules, $X_{\text{eth}} = N_{\text{eth}}/(N_{\text{eth}} + N_w)$. As common, periodic boundary conditions were used. Temperature and pressure control was provided by the V-rescale thermostat and Parrinello-Rahman barostat with τ_T = 0.5 ps and τ_P = 2.0 ps, the timestep was 0.002 ps. The value of $4.5 \cdot 10^{-5}$ bar^{-1} was used for the compressibility of mixtures.

The non-bonded interactions were cut-off at 1.1 nm, whereas the long-range electrostatic interactions were handled by the particle mesh Ewald method implemented in the GROMACS software package (fourth order, Fourier spacing equal to 0.12) with the precision 10^{-5}. The van der Waals correction terms to the energy and pressure were used. In order to maintain the geometry of water molecules and ethanol intra-molecular bonds rigid, the LINCS algorithm was used.

After preprocessing and equilibration, consecutive simulation runs, each for not less than 10 ns, with the starting configuration being the last configuration from the previous run, were performed to obtain trajectories for the data analysis. The results for each property were obtained by averaging over 7–10 production runs.

3. Results and discussion

3.1. Density of ethanol-water mixtures on composition

As we mentioned in the introductory section, there were several experimental reports concerning the density of water-ethanol mixtures upon changing composition. We used experimental data at room temperature T = 298.15 K, and at atmospheric pressure [36, 37].

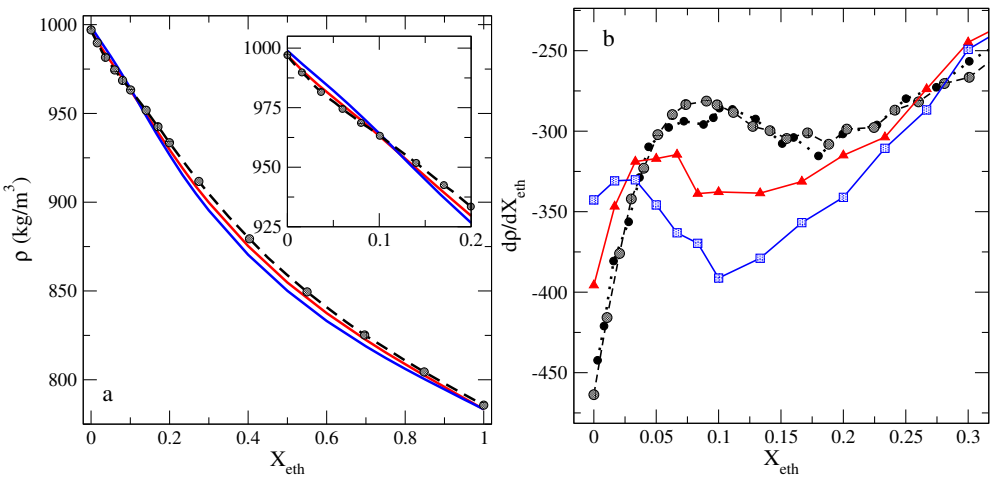

Figure 1. (Color online) Panel a: Composition dependence of density of water-ethanol mixtures from the NPT MD simulations of TIP4P/2005-TraPPE model (solid red line), SPC/E-TraPPE model (solid blue line), in comparison with the experimental data (dashed lines with circles) at T = 298.15 K [36]. The inset provides an enhanced view of density changes at low ethanol concentrations. Panel b: Derivative of density by ethanol concentration at low X_{eth}, experimental data from [36] — circles with dotted line, [37] — circles with dashed line, TIP4P/2005-TraPPE model — red triangles, SPC/E-TraPPE — blue squares.

Both combinations of models of this study describe the dependence of density on X_{eth} quite well. Pure ethanol density is ≈ 783.5 kg/m^3 close to the experimental value 785.2 [36] or 785.7 kg/m [37]. The most pronounced deviation of simulation data from experimental results are observed at intermediate compositions, but inaccuracy is not big, however (figure 1a). At a low ethanol concentration, both models capture the maximum of the derivative of density on X_{eth}, figure 1b. This behavior describes the peculiarity of mixing of a small amount of ethanol in the medium of water species. It witnesses the

contraction of the mixture volume and is commonly attributed to the hydrophobic effect. We discuss this issue more in detail herein below.

3.2. Excess mixing volume

It is important not only to describe the trends of behavior of a given property on composition, but to capture correctly the deviation from ideality as well. These insights follow, for example, from the behavior of the excess density or the excess mixing volume. The excess mixing volume is defined as follows, $\Delta V_{\text{mix}} = V_{\text{mix}} - X_{\text{eth}} V_{\text{eth}} - (1 - X_{\text{eth}}) V_w$, where V_{mix}, V_{eth} and V_w refer to the molar volume of the mixture and of the individual components, ethanol and water, respectively.

Experimental data show that ΔV_{mix} is negative and exhibits a minimum at $X_{\text{eth}} \approx 0.4$, figure 2. The simulation results show qualitatively similar trends of behavior. A comparison between the experiment and simulations with TIP4P-2005-TraPPE model can be termed as quite satisfactory. The SPC/E-TraPPE model is less accurate concerning the description of geometric aspects of mixing of species. In this projection of the equation of state, a single peculiar point on composition is well observed.

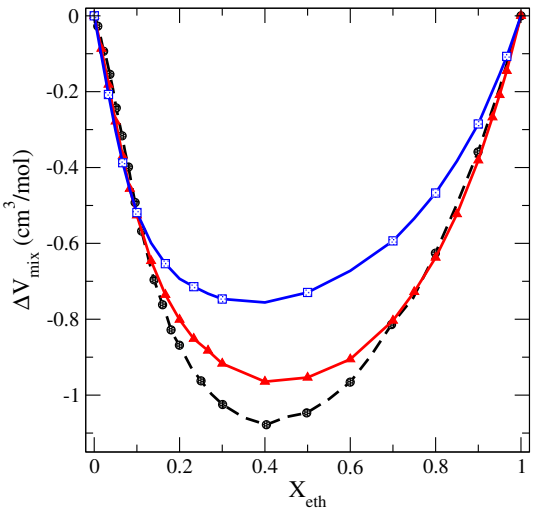

Figure 2. (Colour online) A comparison of the composition dependence of the excess mixing volume of water-ethanol mixtures for models as in figure 1 with the experimental data of [36]. The experimental data are given by black dashed line with circles; red line with triangles and blue line with squares correspond to TIP4P/2005-TraPPE model and SPC/E-TraPPE model, respectively. The results refer to 298.15 K and atmospheric pressure.

In order to discern the contributions of each species into the excess molar volume and to obtain deeper insights into the geometric aspects of mixing on composition, both from experiments and simulations, one can resort to the notion of the apparent molar volume of species rather than the excess molar volumes. The apparent molar volume for each species according to the definition is [38]: $V_\phi^{(w)} = V_w + \Delta V_{\text{mix}}/(1 - X_{\text{eth}})$ and $V_\phi^{(\text{eth})} = V_{\text{eth}} + \Delta V_{\text{mix}}/X_{\text{eth}}$. We elaborated the experimental density data from [36] and the results from our simulations to construct the plots shown in panels a and b of figure 3. These plots confirm that the TIP4P-2005-TraPPE model provides a quite reasonable description of the composition behavior for $V_\phi^{(\text{eth})}$ in water-rich mixtures in the entire composition range. The minimum of $V_\phi^{(\text{eth})}$ is predicted at a slightly lower ethanol concentration, $X_{\text{eth}} \approx 0.0667$, in comparison with the experimental result, $X_{\text{eth}} \approx 0.1$. On the other hand, the SPC/E-TraPPE model is less accurate in this respect. Apparently, the minimum of $V_\phi^{(\text{eth})}$ exists at a much lower ethanol concentration for this model. Concerning the apparent molar volume of water (panel b of figure 3), we observe that the TIP4P-2005-TraPPE model leads to more accurate predictions.

This kind of composition behavior of apparent molar volumes of ethanol species in water-rich mixtures

can be related to the experimental results for abnormal intensity of scattered light [10–12]. Experimental evidence of a peculiar point at $X_{\mathrm{eth}} \approx 0.12$ corresponding to the largest concentration fluctuations is commonly interpreted in terms of the formation of ethanol clusters and changes of their shape. From the thermodynamic point of view, the minimum of the apparent molar volume of ethanol indicates the hydrophobic effect at this composition interval.

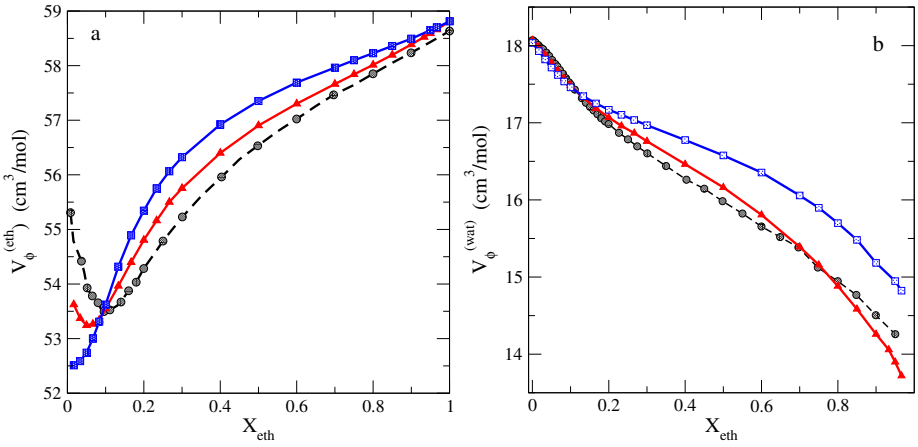

Figure 3. (Colour online) A comparison of the composition dependence of the apparent molar volumes of ethanol and water species from simulations, with the experimental data [36] at 298.15 K. The nomenclature of lines and symbols as in figure 2.

It is worth mentioning that some combinations of alcohol and water models, in spite of apparently accurate description of density and the excess mixing volume, do not capture the minimum of the excess apparent volume of alcohol and do not correctly reproduce the temperature dependence of hydrophobic effect [39]. This issue requires additional studies for water-ethanol mixtures.

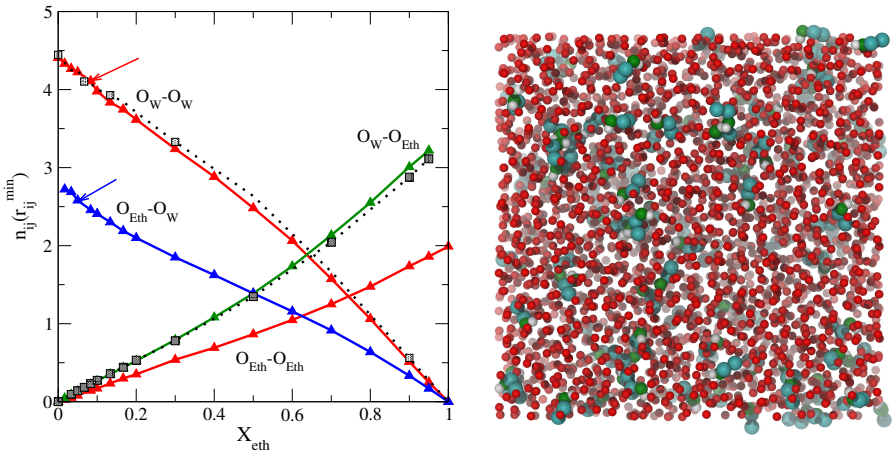

Figure 4. (Colour online) Left-hand panel: composition dependence of the first coordination number of oxygens belonging to water and to ethanol species at 298.15 K. The solid lines with symbols and dotted line with symbols correspond to TIP4P/2005-TraPPE and SPC/E-TraPPE model, respectively. Right-hand panel: a snapshot of ethanol molecules typical configuration in water medium (red small circles - O_w) at $X_{\mathrm{eth}} = 0.0333$.

The minimum of the ethanol excess apparent molar volume is observed at small value for X_{eth}, at $X_{\mathrm{eth}} \approx 0.0667$ for TIP4P/2005-TraPPE model. At such conditions, the water-ethanol mixture has got the density quite close to the one of pure water. In order to get insight into the mutual distribution

of particles in such mixtures, we performed calculations of the first coordination number of ethanol and water oxygens. The first coordination number is commonly evaluated by integration of the radial distribution functions up to the first minimum, as follows,

$$n_{ij} = 4\pi\rho_j \int_0^{r_{ij}^{\min}} g_{ij}(R) R^2 \mathrm{d}R, \tag{3.1}$$

where ρ_j is the density of species j and $g_{ij}(r)$ is the corresponding pair distribution function. The anomaly of $V_\phi^{(\mathrm{eth})}$ occurs in highly coordinated mixtures. Namely, the coordination number of water oxygens is ≈4 whereas the ethanol oxygen is surrounded by ≈ 2.5 water oxygens. Moreover, these two first coordination numbers exhibit weak peculiarity at low X_{eth} values (marked by arrows in figure 4, left-hand panel). The snapshot of the configuration of ethanol molecules at $X_{\mathrm{eth}} \approx 0.033$ in right-hand panel of figure 4, illustrates that their distribution is not entirely uniform. Microheterogeneity of the distribution of particles upon changing the composition of the mixture is the subject of many previous studies [23, 24, 31]. This issue is out of scope of the present report, however.

3.3. Energetic aspects of mixing of ethanol and water molecules

Energetic manifestation of mixing trends is commonly discussed in terms of excess mixing enthalpy. We used the experimental results from [6–8] and our simulation data to explore the mixing enthalpy upon composition of water-ethanol mixtures. The results are given in figure 5.

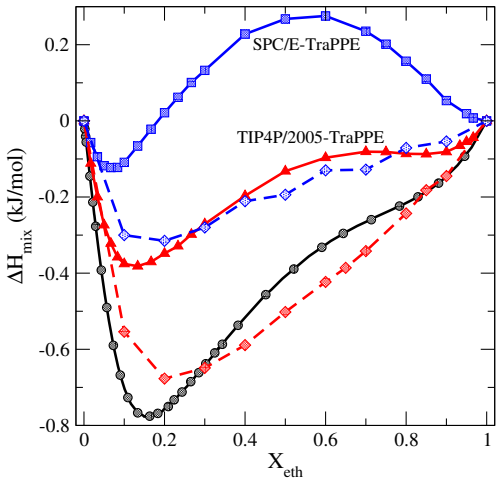

Figure 5. (Colour online) A comparison of the behavior of the excess mixing enthalpy from simulations and experimental data from [6]. The nomenclature of lines and symbols is the same as in figure 2. Two additional curves reproduce the results from [32] with TIP4P/2005 water model (red diamonds) and with SPC/E model (blue diamonds) combined with ethanol model of their own design.

There, we observe that the TIP4P-2005-TraPPE model qualitatively reproduces the shape of experimental behavior. The minimum location and peculiarity of ΔH_{mix} at high values of X_{eth} agree reasonably well with the experimental trends. The absolute values from TIP4P-2005-TraPPE model for ΔH_{mix} are underestimated, however. The SPC/E-TraPPE model predictions are not satisfactory for ΔH_{mix}. Large scattering of data for ΔH_{mix} upon composition for water-ethanol mixtures is comprehensively documented in figure 2 of [23] and in figure 22 of [32]. Moreover, the absolute values for ΔH_{mix} from the study of Wensink et al. [19] are almost twice larger than the experimental ones. In order to elucidate the reasons of this kind of discrepancy of modelling and experiment, it is worth to resort to the partial excess

molar enthalpies. They result from the excess mixing enthalpy, $\Delta H_{\rm mix}$ as follows [38],

$$h_w^{\rm ex} = \Delta H_{\rm mix} + X_{\rm eth} \left(\frac{\partial \Delta H_{\rm mix}}{\partial X_w} \right)\Big|_{P,T}, \tag{3.2}$$

$$h_{\rm eth}^{\rm ex} = \Delta H_{\rm mix} - X_w \left(\frac{\partial \Delta H_{\rm mix}}{\partial X_w} \right)\Big|_{P,T}, \tag{3.3}$$

where, $X_w = 1 - X_{\rm eth}$.

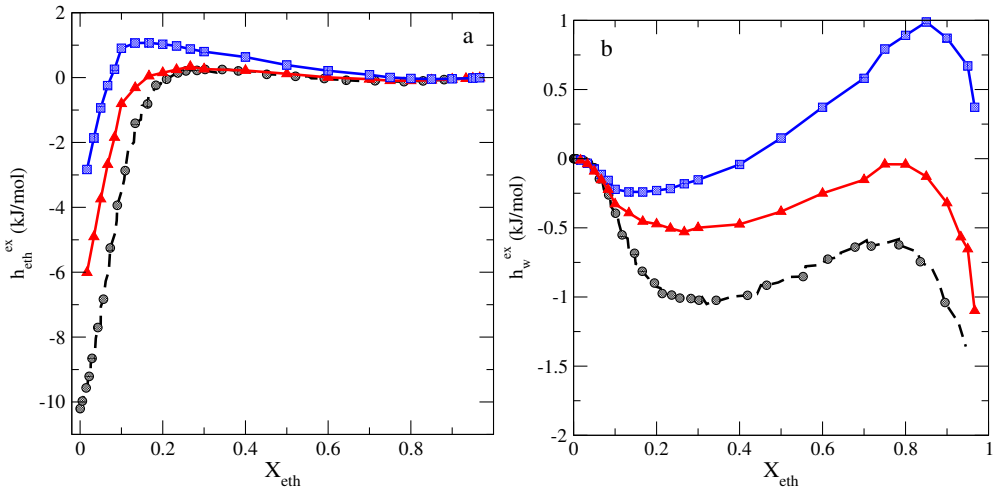

Figure 6. (Colour online) A comparison of the behavior of the partial molar excess enthalpy from simulations and experimental data from [7, 8]. The nomenclature of lines and symbols is the same as in figure 2.

In general terms, the computer simulation predictions for $h_{\rm eth}^{\rm ex}$ are reasonable, as we see from figure 6a. On the other hand, the shape of behavior of $h_w^{\rm ex}$ reproduces the experimental behavior as well, figure 6b. However, the absolute values of this property substantially differ from the experimental data. Still, the TIP4P-2005-TraPPE model provides a satisfactory description of the energetic trends of mixing of ethanol and water species.

3.4. On the predictions from fluctuations

Now, we would like to turn our attention to a set of properties that proceed from fluctuations. These quantities and their composition dependence are less frequently discussed in literature compared to the excess mixing volume and enthalpy and require more computational efforts, see, e.g., [40] for pure water.

The thermal expansion coefficient, α_P, and isothermal compressibility, κ_T,

$$\alpha_P = \frac{1}{V}\left(\frac{\partial V}{\partial T}\right)|_P = -\frac{1}{\rho}\left(\frac{\partial \rho}{\partial T}\right)|_P, \tag{3.4}$$

$$\kappa_T = -\frac{1}{V}\left(\frac{\partial V}{\partial P}\right)|_T = \frac{1}{\rho}\left(\frac{\partial \rho}{\partial P}\right)|_T, \tag{3.5}$$

are obtained as block averages from the set of runs. They are plotted in two panels of figure 7. One can conclude that the models used in simulations provide a qualitatively correct description of these properties upon composition. However, in both cases, the absolute values of α_P and κ_T are overestimated in comparison with the experimental data. The TIP4P-2005-TraPPE model is better than the SPCE/E-TraPPE one. It is important to mention that the κ_T dependence on ethanol concentration from simulations captures the hydrophobic effect, in close similarity to the behavior of the density shown previously in figure 1b and in figure 3a for the apparent molar volume of ethanol.

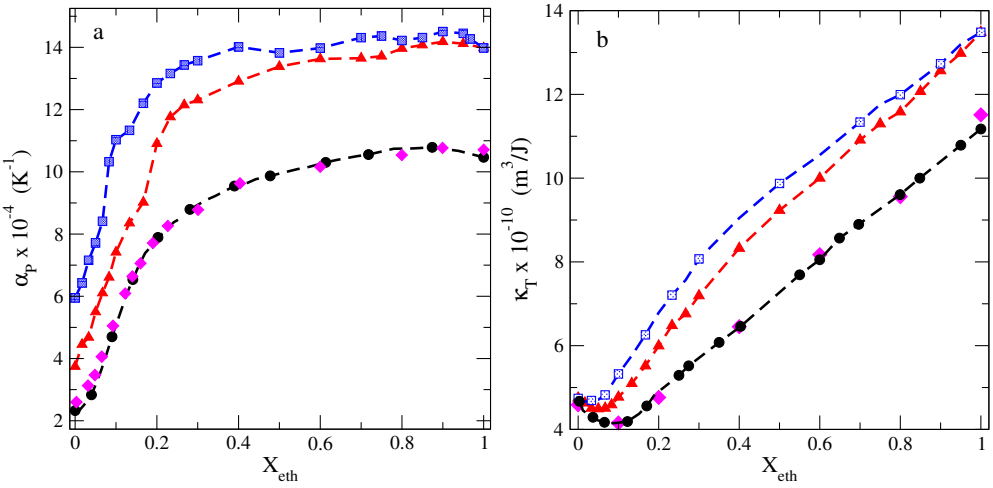

Figure 7. (Colour online) A comparison of the composition dependence of the coefficient of the isobaric thermal expansion, α_P, and isothermal compressibility, κ_T, in panels a and b, respectively, with the experimental data. Panel a: circles and diamonds are from [36] and from [37], respectively. Panel b: circles and diamonds are from [36] and from [41], respectively.

The adiabatic bulk modulus, which is the inverse of adiabatic compressibility, from simulations and experimental results is shown in figure 8. These data are important because the isoentropic compressibility is related to the speed of sound via Newton-Laplace equation, see, e.g., [42]. Moreover, the isoentropic compressibility, κ_S follows from the combination of other fluctuation-type properties, $\kappa_S = \kappa_T - T\alpha^2/\rho C_P$, where C_P is the constant pressure heat capacity. It was shown recently [42] that simulations of TIP4P-2005-TraPPE model predict the composition dependence of the speed of sound for water-ethanol mixtures reasonably well (figure 1 of that reference). The maximum value of the speed of sound is reproduced at a slightly lower X_{eth}, in comparison with the experiment [43]. Our comparison with the same set of experimental data describes similar trends. In addition, we observe that the SPCE/E-TraPPE model captures the maximum at even lower X_{eth} than the TIP4P/2005-TraPPE one.

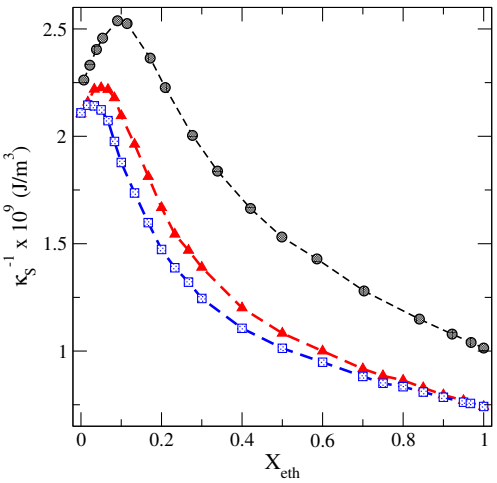

Figure 8. (Colour online) A comparison of the composition dependence of adiabatic bulk modulus, κ_S^{-1}, with the experimental data. Circles are from [43].

We would like to conclude this subsection by the presentation of the simulation results for the constant pressure heat capacity. These are collected as averages for a set of runs without applying any

correction due to the density of states. The results for the dependence of heat capacity and the excess heat capacity upon ethanol concentration are given in figure 9. The heat capacity values are overestimated in comparison with the experimental result but the dependence of the excess heat capacity from simulations is reasonably good. Both water models combined with TraPPE ethanol yield the results of comparable quality.

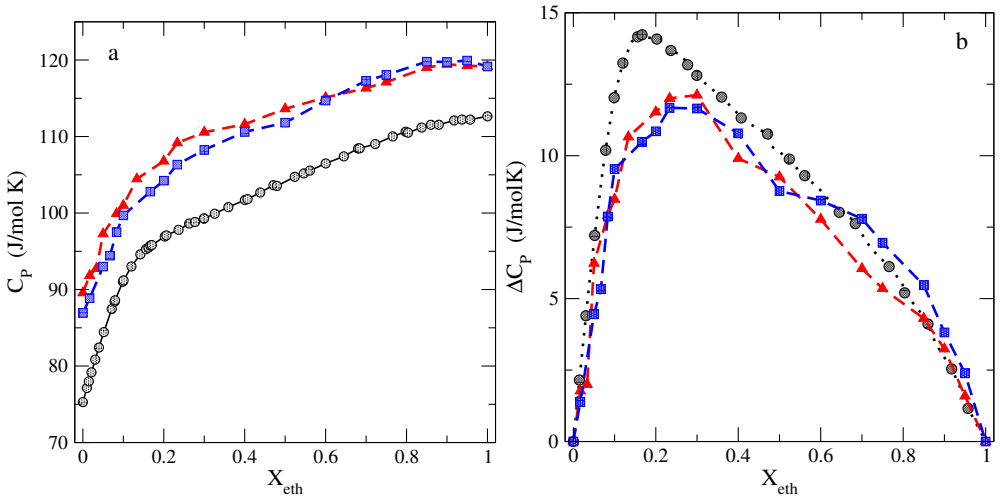

Figure 9. (Colour online) Panels a and b: A comparison of the composition dependence of the heat capacity and the excess molar heat capacity from simulations, with the experimental data [5] at 298.15 K. The nomenclature of lines and symbols is the same as in figure 2.

We would like to note here that some of these properties were explored by simulations of the TraPPE ethanol model combined with modified Fw-SPC water model [44]. According to figure S1 of this work, the coefficient of thermal expansion is closer to the experimental observations compared to our data. On the other hand, again from figure S1, it follows that the minimum of isothermal compressibility at low ethanol concentrations is not captured appropriately. Finally, computer simulation predictions for the heat capacity [44] are of similar quality as our results.

3.5. Self-diffusion coefficients of ethanol and water molecules

One of the most popular properties to test models for binary mixtures is the self-diffusion coefficients of species. They can be obtained from the mean square displacement of particles or from calculations of the velocity articulation functions. We calculate the self-diffusion coefficients, D_i (i = w, eth), by the former route, via the Einstein relation,

$$D_i = \frac{1}{6} \lim_{t\to\infty} \frac{\mathrm{d}}{\mathrm{d}t} |\mathbf{r}_i(\tau + t) - \mathbf{r}_i(\tau)|^2, \tag{3.6}$$

where τ denotes the time origin. Default settings of GROMACS were used for the separation of the time origins. The experimental data were taken from [45]. According to the experiments, the self-diffusion coefficient of water species decreases in magnitude starting from pure water value (at $X_{\mathrm{eth}} = 0$) and reaches minimum at $X_d \approx 0.5$, figure 10a. Next, for higher values of X_{eth}, D_w does not change much. Apparently, the behavior of $D_i(X_{\mathrm{eth}})$ is determined by the evolution of density of the mixture and by hydrogen bonding between all species, figure 10b. Simulation predictions for D_w show a satisfactory agreement with experimental trends in the entire composition interval, if the TIP4P-2005-TraPPE model is used. The SPC/E model overestimates the self-diffusion coefficient for water and consequently the values for D_w are overestimated for mixture at all compositions studied. The shape of $D_w(X_{\mathrm{eth}})$ curve is however similar to the experimental behavior and to the TIP4P-2005-TraPPE model predictions. The TraPPE model for ethanol does not describe the pure ethanol self-diffusion coefficient accurately. In consequence, only the

trends of behavior for $D_{\mathrm{eth}}(X_{\mathrm{eth}})$ are qualitatively correct. There is a minimum value at $X_{\mathrm{eth}} \approx 0.2$ from the experimental data. The TIP4P-2005-TraPPE shows a minimum value at $X_{\mathrm{eth}} \approx 0.17$ whereas the SPC/E-TraPPE model — at $X_{\mathrm{eth}} \approx 0.27$. In general terms, the TIP4P-2005-TraPPE predictions are better.

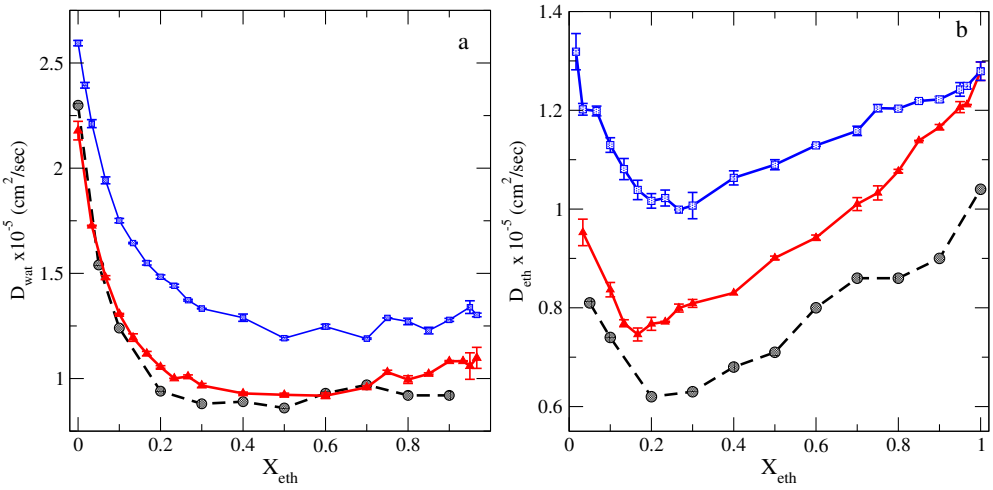

Figure 10. (Colour online) Panels a and b: Composition dependence of the self-diffusion coefficient of water and ethanol, respectively, in water-ethanol mixtures. Experimental data are from [45] (squares). The nomenclature of lines and symbols as in figure 2.

It seems necessary to confirm the present results by using alternative calculations via the velocity auto-correlation functions. In addition, it would be profitable to attempt calculations of the relaxation times and possibly power spectra, because the experimental data are available in the literature. These issues would provide ampler insights into the appropriateness of the force fields to describe the dynamic properties.

3.6. Static dielectric constant of ethanol-water mixtures

The study of dielectric properties of water-alcohol mixtures represents a wide area of research, see, e.g., quite recent contribution [44], as an example concerned with some interesting issues for water-ethanol mixtures. Here, we would like to focus solely on the calculation of the static dielectric constant. The long-range, asymptotic behavior of correlations between molecules possessing a dipole moment is described by the dielectric constant, ε. It is calculated from the time-average of the fluctuations of the total dipole moment of the system [46] as follows,

$$\varepsilon = 1 + \frac{4\pi}{3k_{\mathrm{B}}TV}(\langle \mathbf{M}^2 \rangle - \langle \mathbf{M} \rangle^2), \tag{3.7}$$

where k_{B} is the Boltzmann constant and V is the simulation cell volume. Technical aspects of calculations were commented by us in several publications, see, e.g., [47]. The experimental data are taken from [48, 49]. The dielectric constant, ε, and the excess dielectric constant, $\Delta\varepsilon$ (defined similarly to excess molar volume or enthalpy, see section 3.2) are plotted in figure 11. The dielectric constant decreases from a high value for water to a much lower value for pure ethanol, figure 11a.

Computer simulations of the models in question underestimate ε in the entire composition interval. On the water-rich side, the problem is that both water models in question underestimate ε of pure water. This issue can be solved by considering the TIP4P/ε model [50]. On the ethanol-rich side, the problem is that the TraPPE ethanol model underestimates ε of pure ethanol. The curve of similar quality follows from the simulations of TraPPE ethanol combined with Fw-SPC water, which is given in figure 6a of [44]. A better ethanol model is required to mitigate this deficiency. One possibility is to involve the primary alcohols model designed in the laboratory of J. J. de Pablo [51]. We are aware of the successful

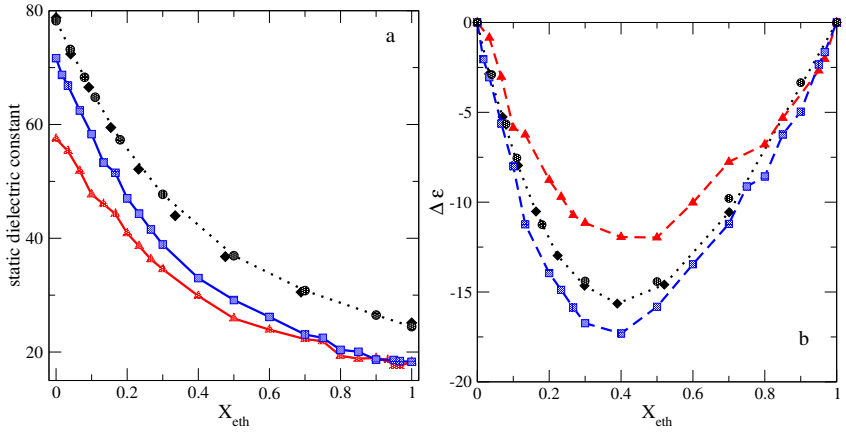

Figure 11. (Colour online) Panels a and b: A comparison of the composition dependence of the dielectric constant and the excess dielectric constant, respectively, from simulations, with the experimental data ([48] — diamonds) at 298.15 K. The nomenclature of lines and symbols is the same as in figure 2. Another set of data is from [49] (circles).

parametrization of the dielectric constant of propanol-water mixtures, [52], by using this model. For ethanol this issue has not been solved so far.

In spite of inaccuracy of the absolute values for the dielectric constant, the shape of $\varepsilon(X_{\text{eth}})$ is quite reasonable, figure 11b. The maximum deviation from ideality is observed at $X_{\text{eth}} \approx 0.4$, as in experiments. The SPC/E-TraPPE results are closer to the experimental curve than the TIP4P/2005-TraPPE ones. Still, in general terms the agreement of simulation data and experiment can be termed as satisfactory.

3.7. Surface tension of ethanol-water mixtures on composition

Our final remarks concern the behavior of the surface tension of ethanol-water mixtures. This research topic has long history as documented in [53]. Recent studies refer to experimental characterization of this liquid-vapor interface [54, 55] and its study using molecular dynamics simulations [18].

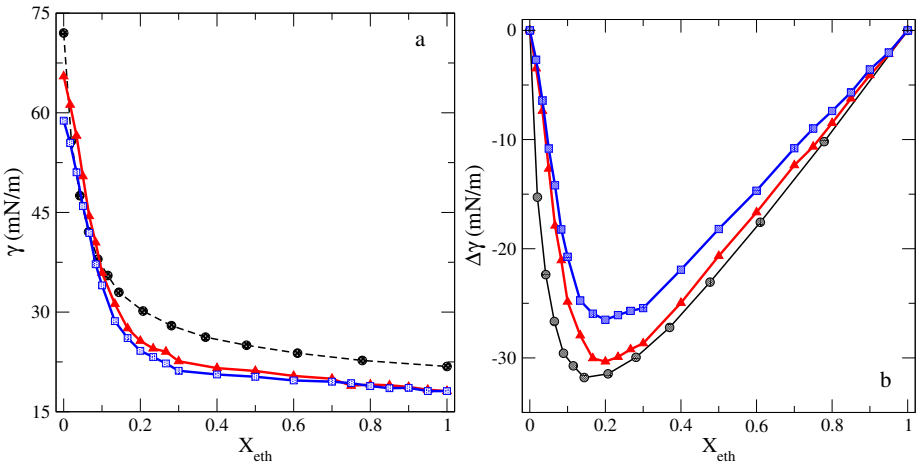

Figure 12. (Colour online) Panels a and b: A comparison of the composition dependence of the surface tension and the excess surface tension, respectively, from simulations, with the experimental data [57] at 298.15 K. The nomenclature of lines and symbols is the same as in figure 2.

The surface tension calculations at each composition were performed by taking the final configuration

of particles from the isobaric run. However, it is well known that the cutoff distance should be increased to obtain accurate values for surface tension. After short trials, we chose, $r_c = 1.4$ nm, in what follows. Next, the box edge along z-axis was extended by a factor of 3, generating a rectangular box with liquid slab and two liquid-mixture-vacuum interfaces in the $x - y$ plane, in close similarity to the procedure used in [56]. The total number of molecules is sufficient to yield an area of the $x - y$ face of the liquid slab sufficiently big. The elongation of the liquid slab along z-axis is satisfactory as well. The executable file was modified by deleting a fixed pressure condition preserving the V-rescale thermostatting with the same parameters as in the NPT runs. Other corrections were not employed.

The values for the surface tension, γ, follow from the combination of the time averages for the components of the pressure tensor,

$$\gamma = \tfrac{1}{2} L_z \langle [P_{zz} - \tfrac{1}{2}(P_{xx} + P_{yy})] \rangle, \tag{3.8}$$

where P_{ij} are the components of the pressure tensor along i, j axes, and $\langle \ldots \rangle$ denotes the time average. We performed a set of runs at a constant volume, each piece of 10 ns, and obtained the result for γ by taking the block average. The experimental results were taken from [57]. The data show that the surface tension rapidly decreases from the pure water value at $X_{\text{eth}} = 0$ till $X_{\text{eth}} \approx 0.25$. Next, at higher X_{eth}, the values for γ decrease more slowly, the curve behaves almost linearly in that interval of compositions, panel a of figure 12. At $X_{\text{eth}} = 0$, we have $\gamma \approx 65.5$ for TIP4P/2005 water and $\gamma \approx 58.8$ for SPC/E water model without long-range correction, in agreement with data 65.3 and 60.2, reported in [58], respectively. For TraPPE ethanol, $X_{\text{eth}} = 1$, we obtained $\gamma \approx 18.1$, in close similarity to the points in figure 7 of [59]. In the interval of not small ethanol concentration, $X_{\text{eth}} > 0.15$, the absolute values for γ from simulations are underestimated compared to experimental data. It is difficult to expect that inclusion of long-range corrections would mitigate this problem. Rather, one should search for parametrization of the ethanol model.

The excess surface tension from experiment exhibits minimum at $X_{\text{eth}} \approx 0.17$. Two models in question behave similarly for water-rich mixtures. The decay of γ is a bit better reproduced by the TIP4P-2005-TraPPE model, in comparison with SPC/E -TraPPE one. It is of interest to explore the structure of the interface in terms of density profiles of the species. Previously, these profiles were reported in [18, 53]. Namely, in [18], the dependence of the density profiles on water-ethanol mixture composition was studied. We use a similar type of presentation of the profiles in figure 13. Besides, the properties of the air/solution interface were examined by Tarek et al. [53] at single, 0.1 M, composition of ethanol-water mixture.

The left-hand panels of figure13 refer to TIP4P/2005-TraPPE model, whereas two right-hand panels show similar results but for SPC/E-TraPPE model. At a low concentration of ethanol species in the bulk phase, $X_{\text{eth}} = 0.03$, one can see that the ethanol molecules segregate from the bulk to the interface (panel c of figure 13) and form a monolayer. In order to explain the changes of the location of the monolayer, we refer to the panel a of figure14. At a very low X_{eth}, $X_{\text{eth}} = 0.0167$, the interface composition is dominated by water species. However, already at $X_{\text{eth}} = 0.0833$, segregation of ethanol molecules from the bulk becomes stronger, so that these species overcome water concentration within the interface region.

A certain degree of depletion of water molecules from the bulk to the interfaces is observed in the concentration interval, $0.0833 < X_{\text{eth}} < 0.5$, according to the TIP4P/2005-TraPPE model (panel a of figure 13). By contrast, these trends are much weaker within the SPC/E-TraPPE model (panel b of figure 13). At a higher ethanol concentration in the bulk, e.g., $X_{\text{eth}} = 0.5$, the interface composition is dominated by the ethanol molecules, figure 13a and figure 14b.

This set of results complement the previous observations made in [18, 53] concerning composition evolution of the liquid-vapor interface of water-ethanol mixtures.

4. Summary and conclusions

Some time ago, we undertook rather comprehensive studies of the composition evolution of the properties of water-methanol mixtures [34, 39, 60]. In the present work, we explore water-ethanol systems with the same methodology but using the non-polarizable, united atom ethanol TraPPE model in conjunction with the TIP4P-2005 and SPC/E water models.

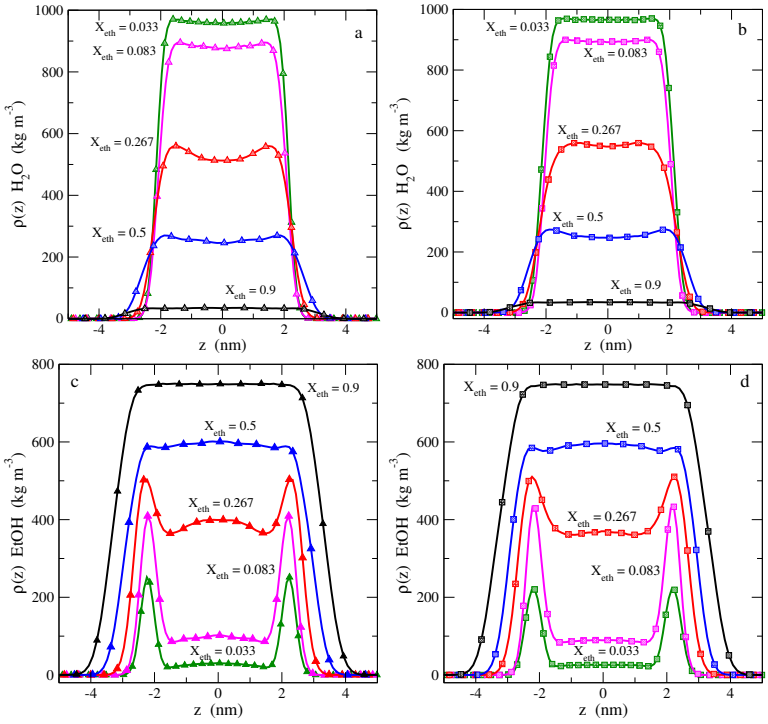

Figure 13. (Colour online) Mass density profiles of water species through vapor-liquid interface on composition for TIP4P-2005-TraPPE (panel a) and SPC/E-TraPPE model (panel b). Density profiles of ethanol species for TIP4P-2005-TraPPE (panel c) and SPC/E-TraPPE model (panel d). Triangles refer to TIP4P-2005-TraPPE profiles whereas the squares are for SPC/E-TraPPE model.

A set of novel findings concerning a wide range of properties of these models were obtained and discussed in comparison to experimental data. Namely, we obtained the excess apparent molar volumes and excess partial molar enthalpies. Analyses of these properties permitted us to capture an anomalous behavior observed at a low ethanol molar fraction in agreement with experimental results. In addition, we described the composition dependence of the properties coming from calculations of fluctuations. The self-diffusion coefficients of species were obtained. Next, the static dielectric constant was calculated and compared with experimental results. Our final focus was on elucidation of the behavior of the surface tension on the composition of water-ethanol mixtures and of the excess surface tension. The density profiles of the species through the liquid-vapor interface are discussed. All the trends were compared with experimental data. A detailed validation of the predictions of the properties resulting from a set of models for water-ethanol solutions permits to make conclusions w.r.t. their applicability. We have not observed the trends that contradict the experimental findings. In general terms, the TIP4P/2005-TraPPE model seems to be superior in comparison with SPC/E-TraPPE model. This latter model is better for the description of the dielectric constant only. However, the TIP4P/2005 can be replaced by TIP4Pε model to mitigate the problem. Various excess mixing properties are better decribed than the corresponding absolute values. Still, it seems that the improvement of agreement with experimental data can be reached only by designing a more accurate ethanol model.

Finally, we would like to enlist a few missing elements to extend our knowledge of the properties of water-ethanol mixtures. It would be profitable to explore various velocity auto-correlation functions to enhance the understanding of dynamic properties, as well as the frequency dependent dielectric constant to better understand the dielectric properties. We were unable to extract useful pieces of information from the Kirwood factors, for the moment. As it was mentioned in the introduction, all the issues concerned with the composition evolution of the microscopic structure and hydrogen bonds network will be reported elsewhere.

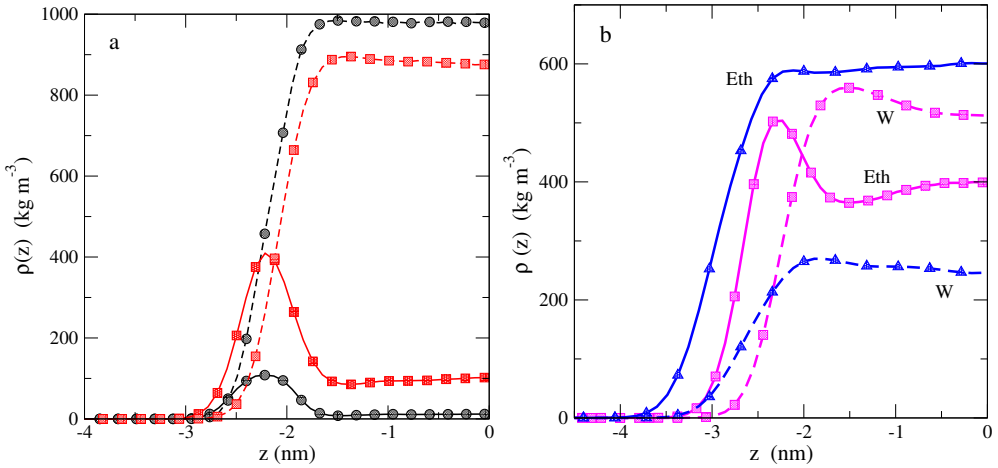

Figure 14. (Colour online) A comparison of the mass density profiles of the species through liquid-vapor interface with TIP4P/2005-TraPPE model at different compositions. In panel a, $X_{\mathrm{eth}} = 0.0167$ (black lines and circles), $X_{\mathrm{eth}} = 0.0833$ (red lines and squares). In panel b, $X_{\mathrm{eth}} = 0.267$ (magenta lines and squares) and $X_{\mathrm{eth}} = 0.5$ (blue lines and triangles). Profiles of water and of ethanol species are given by dashed and solid lines, respectively.

Moreover, a detailed comparison of the predictions coming out from united atom and all atom force fields for water-alcohol mixtures is still missing at present. Recent, quite general analyses of the mixing trends were given in [61] by using Monte Carlo simulations. Qualitative agreement of the results of models with a different degree of sophistication with experimental behavior was observed. Nevertheless, these findings require an extension for specific systems in future work. On the other hand, some recent efforts were focused on the improvement of the description of thermodynamic and other properties by multi-step parametrization of united atom models for simple alcohols with non-polarizable water models [62]. Again, extensive additional work is needed to reach definite conclusions concerning the accuracy of the constructed force fields.

It is worth mentioning that the solvation of complex molecules in water-ethanol mixtures was the subject of several simulations and experimental studies, see, e.g., [18, 63–65]. Some important aspects within this research area are under study in our laboratory. Namely, along the lines considered in the report from Scotch whisky research institute [18], we intend to analyze the trends of the smell of beverages of Mexican origin, see, e.g., [66], by using computer simulation techniques. Concerning the experimental work focused on the properties of molecules that are promising for medical applications [65], our present interest is in clustering of curcumin molecules in water-ethanol mixtures, as an extension of our recent contribution [67]. Progress along these research lines will be reported elsewhere.

Acknowledgements

O.P. acknowledges helpful discussions with Dr. Laszlo Pusztai concerning experimental measurements of the structure of water-ethanol mixtures.

References

1. Stewart G. W., Morrow R. M., Phys. Rev., 1927, **30**, 232, doi:10.1103/PhysRev.30.232.
2. Raman C .V., Sogani C. M., Nature, 1927, **119**, 601, doi:10.1038/120514a0.
3. Harris K. R., Newitt P. J., J. Phys. Chem. B, 1998, **102**, 8874, doi:10.1021/jp9820370.
4. Petong P., Pottel R., Kaatze U., J. Phys. Chem. A, 2000, **104**, 7420, doi:10.1021/jp001393r.
5. Benson G. C., D'Arcy P. J., Kiyohara O., J. Solution Chem., 1980, **9**, 931, doi:10.1007/BF00646404.

6. Costigan M. J., Hodges L. J., Marsh K. N., Stokes R. H., Tuxford C. W., Aust. J. Chem., 1980, **33**, 2103, doi:10.1071/CH9802103.
7. Liltorp K., Westh P., Koga Y., Can. J. Chem., 2005, **83**, 420, doi:10.1139/V05-050.
8. Tanaka S. H., Yoshihara H. I., Wen-Chi Ho A., Lau F. W., Westh P., Koga Y., Can. J. Chem., 1996, **74**, 713 doi:10.1139/v96-077.
9. Grolier J.-P. E., Wilhelm E., Fluid Phase Equilib., 1981, **6**, 283, doi:10.1016/0378-3812(81)85011-X.
10. Sato M., Ike Y., Kano J., Kojima S., AIP Conf. Proc., 2006, **832**, 291, doi:10.1063/1.2204509.
11. Gotsulskiy V. Ya., Malomuzh N. P., Chechko V. E., Russ. J. Phys. Chem. A, 2015, **9**, 207, doi:10.1134/S0036024415020119.
12. Chechko V. E., Gotsulsky V. Ya., Malomuzh M. P., Condens. Matter Phys., 2013, **16**, 23006, doi:10.5488/CMP.16.23006.
13. Vega C., Abascal J. L. F., Phys. Chem. Chem. Phys., 2011, **13**, 19663, doi:10.1039/C1CP22168J.
14. Gonzalez-Salgado D., Vega C., J. Chem. Phys., 2016, **145**, 034508, doi:10.1063/1.4958320.
15. Saiz L., Padro J. A., Guardia E., J. Phys. Chem. B, 1997, **101**, 78, doi:10.1021/jp961786j.
16. Padro J. A., Saiz L., Guardia E., J. Mol. Struct., 1997, **416**, 243, doi:10.1016/S0022-2860(97)00038-0.
17. Zangi R., ACS Omega, 2018, **3**, 18089, doi:10.1021/acsomega.8b03132.
18. Shuttleworth E. E., Apostolo R. F. G., Camp P. J., Conner J. M., Harrison B., Jack F., Clark-Nicolas J., J. Mol. Liq., 2023, **383**, 122152, doi:10.1016/j.molliq.2023.122152.
19. Wensink E. J. W., Hoffmann A. C., van Maaren P. J., van der Spoel D., J. Chem. Phys., 2003, **119**, 7308, doi:10.1063/1.1607918.
20. Berendsen H. J. C., Grigera J. R., Straatsma T. P., J. Phys. Chem., 1987, **91**, 6269, doi:10.1021/j100308a038.
21. Abascal J. L. F., Vega C., J. Chem. Phys., 2005, **123**, 234505, doi:10.1063/1.2121687.
22. Mijaković M., Kežić B., Zoranić L., Sokolić F., Asenbaum A., Pruner C., Wilhelm E., Perera A., J. Mol. Liq., 2011, **164**, 66, doi:10.1016/j.molliq.2011.06.009.
23. Mijaković M., Polok K. D., Kežić B., Sokolić F., Perera A., Zoranić L., Mol. Simul., 2015, **41**, 699, doi:10.1080/08927022.2014.923567.
24. Požar M., Lovrinčević B., Zoranić L., Primorać T., Sokolić F., Perera A., Phys. Chem. Chem. Phys., 2016, **18**, 23971, doi:10.1039/C6CP04676B.
25. Gereben O., Pusztai L., J. Phys. Chem B, 2015, **119**, 3070, doi:10.1021/jp510490y.
26. Gereben O., Pusztai L., J. Mol. Liq., 2016, **220**, 836, doi:10.1016/j.molliq.2016.05.035.
27. Pothoczki S., Pusztai L., Bakó I., J. Phys. Chem. B, 2018, **122**, 6790, doi:10.1021/acs.jpcb.8b02493.
28. Jorgensen W. L., J. Phys. Chem., 1986, **90**, 1276, doi:10.1021/j100398a015.
29. Jorgensen W. L., Maxwell D., Tirado-Rives S., J. Am. Chem. Soc., 1996, **118**, 11225, doi:10.1021/ja9621760.
30. Chen B., Potoff J. J., Siepmann J. I., J. Phys. Chem. B, 2001, **105**, 3093, doi:10.1021/jp003882x.
31. Ghosh R., Bagchi B., J. Phys. Chem. B, 2016, **120**, 12568, doi:10.1021/acs.jpcb.6b06001.
32. Guevara-Carrion G., Vrabec J., Hasse H., J. Chem. Phys., 2011, **134**, 074508, doi:10.1063/1.3515262.
33. Zhong Y., Patel S., J. Phys. Chem., 2009, **113**, 767, doi:10.1021/jp807053p.
34. Galicia-Andrés E., Pusztai L., Temleitner L., Pizio O., J. Mol. Liq., 2015, **209**, 586, doi:10.1016/j.molliq.2015.06.045.
35. Spoel D., Lindahl E., Hess B., Groenhof B., Mark A. E., Berendsen H. J. C., J. Comput. Chem., 2005, **118**, 1701, doi:10.1002/jcc.20291.
36. Pečar D., Doleček V., Fluid Phase Equilib., 2005, **230**, 36, doi:10.1016/j.fluid.2004.11.019.
37. Hervello M. F., Sanchez A., J. Chem. Eng. Data, 2007, **52**, 752, doi:10.1021/je060335h.
38. Torres R. B., Marchiore A., Volpe P., J. Chem. Thermodyn., 2006, **38**, 526, doi:10.1016/j.jct.2005.07.012.
39. Cruz Sanchez M., Aguilar M., Pizio O., Condens. Matter Phys., 2020, **23**, 34601, doi:10.5488/CMP.23.34601.
40. Alejandre J., Chapela G. A., Saint-Martin H., Mendoza N. Phys. Chem. Chem. Phys., 2011, **13**, 19728, doi:10.1039/c1cp20858f.
41. Tanaka Y., Yamamoto T., Satomi Y., Kubota H., Makita T., Rev. Phys. Chem. Jpn., 1977, **47**, No. 1, 12–24.
42. Ashbaugh H. S., Barnett J. W., Saltzman A., Langrehr M. E., Houser H., J. Chem. Phys., 2016, **145**, 201102, doi:10.1063/1.4971205.
43. Lara J., Desnoyers J. E., J. Solution Chem., 1981, **10**, 465, doi:10.1007/BF00652081.
44. Cardona J., Sweatman M. B., Lue L., J. Phys. Chem. B, 2018, **122**, 1505, doi:10.1021/acs.jpcb.7b12220.
45. Price W. S., Ide H., Arata Y., J. Phys. Chem. A, 2003, **107**, 4784, doi:10.1021/jp027257z.
46. Neumann M., Mol. Phys., 1983, **50**, 841, doi:10.1080/00268978300102721.
47. Aguilar M., Dominguez H., Pizio O., Condens. Matter Phys., 2022, **25**, 33202, doi:10.5488/CMP.25.33202.
48. Wohlfarth C., In: Static Dielectric Constants of Pure Liquids and Binary Liquid Mixtures. Supplement to IV/6, Lechner M. D. (Ed.), 2008, 3–24. doi:10.1007/978-3-540-75506-7.
49. Sato T., Buchner R., J. Phys. Chem., 2004, **108**, 5007, doi:10.1021/jp035255o.

50. Fuentes-Azcatl R., Alejandre J., J. Phys. Chem. B, 2014, **118**, 1263, doi:10.1021/jp410865y.
51. Khare R., Sum A. K., Nath S. K., de Pablo J. J., J. Phys. Chem. B, 2004, **108**, 10071, doi:10.1021/jp048144d.
52. Mendez-Bermúdez J. G., Dominguez H., Pusztai L., Guba S., Horvath B., Szalai I., J. Mol. Liq., 2016, **219**, 354, doi:10.1016/j.molliq.2016.02.053.
53. Tarek M., Tobias D. J., Klein M. L., Physica A, 1996, **231**, 117, doi:10.1016/0378-4371(95)00450-5.
54. Hyde A. E., Ohshio M., Nguyen C. V., Yusa S., Yamada N. L., Phan C. M., J. Mol. Liq., 2019, **290**, 111005, doi:10.1016/j.molliq.2019.111005.
55. Kirschner J., Gomes A. H. A., Marinho R. R. T., Bjorneholm O., Agren H., Carravetta V., Ottosson N., Naves de Brito A., Bakker H. J., Phys. Chem. Chem. Phys., 2021, **23**, 11568, doi:10.1039/d0cp06387h.
56. Fischer N. M., van Maaren P. J., Ditz J. C., Yildirim A., van der Spoel D., J. Chem. Theory Comput., 2015, **11**, 2938, doi:10.1021/acs.jctc.5b00190.
57. Vazquez G., Alvarez E., Navaza J. M., J. Chem. Eng. Data, 1995, **40**, 611, doi:10.1021/je00019a016.
58. Vega C., de Miguel E., J. Chem. Phys., 2007, **126**, 154707, doi:10.1063/1.2715577.
59. Obeidat A., Al-Salman R., Abu-Ghazleh H., AIP Adv., 2018, **8**, 075321, doi:10.1063/1.5040852.
60. Galicia-Andres E., Dominguez H., Pusztai L., Pizio O., J. Mol. Liq., 2015, **212**, 70, doi:10.1016/j.molliq.2015.08.061.
61. Idrissi A., Jedlovszky P., J. Mol. Liq., 2021, **338**, 116777, doi:10.1016/j.molliq.2021.116777.
62. García-Melgarejo V., Nuñez-Rojas E., Alejandre J., J. Mol. Liq., 2021, **323**, 114576, doi:10.1016/j.molliq.2020.114576.
63. Banerjee S., Ghosh R., Bagchi B., J. Phys. Chem. B, 2012, **116**, 3713, doi:10.1021/jp2085439.
64. Mukherjee S., Deshmukh A. A., Mondal S., Gopal B., Bagchi B., J. Phys. Chem. B, 2019, **123**, 10365, doi:10.1021/acs.jpcb.9b07689.
65. Dias Pereira C. I., de Freitas C. F., Lazarotto Braga T., Braga G., Sonchini Goncalves T., Tessaro A. L., Graton Mikcha J. M., Hioka N., Caetano W., Dyes Pigm., 2022, **197**, 109887, doi:10.1016/j.dyepig.2021.109887.
66. Pineda-Amaya A., Ocaña-Rios I., Garcia-Aguilera M. E., Nolasco-Cancino H., Quiroz-Garcia B., Esturau-Escofet N., Ruiz-Terán F., Chem. Pap., 2021, **75**, 4249, doi:10.1007/s11696-021-01660-5.
67. Patsahan T., Pizio O., Condens. Matter Phys., 2023, **26**, 33605, doi:10.5488/CMP.26.33605.

Моделювання суміші води з етанолом методом молекулярної динаміки. I. Композиційні тенденції в термодинамічних властивостях

Д. Бенавідес Батіста[1], М. Агілар[2], О. Пізіо[2]

[1] Інститут фундаментальних наук та техніки, Автономний університет штату Ідальго, Пачука-де-Сото, Ідальго 42039, Мексика

[2] Інститут хімії, Національний автономний університет Мексики, Сіркуіто Екстеріор, 04510, Мексика

Досліджено композиційну залежність доволі широкого діапазону властивостей рідких сумішей води з етанолом за допомогою комп'ютерного моделювання методом ізобарно-ізотермічної молекулярної динаміки. Розглянуто неполярну модель для молекули етанолу з бази даних TraPPE у поєднанні з моделями води TIP4P-2005 і SPC/E. У наших розрахунках ми обмежуємося значеннями атмосферного тиску 0.1013 МПа та кімнатної температури 298.15 K. Описано композиційні тенденції у поведінці густини, надлишкового об'єму змішування та видимих молярних об'ємів. Також досліджено надлишкову ентальпію змішування і парціальні молярні ентальпії компонент суміші. Крім того, ми досліджуємо коефіцієнт ізобарного теплового розширення, ізотермічну теплоємність, адіабатичний модуль об'ємного стиску та теплоємність при постійному тиску. Також розраховані коефіцієнти самодифузії частинок, статична діелектрична проникність і поверхневий натяг. Ми сподіваємось отримати хороше уявлення про особливості змішування компонент суміші при зміні молярної частки етанолу. Якість прогнозних оцінок критично оцінюється шляхом детального порівняння з експериментальними даними. Насамкінець, обговорюються необхідні вдосконалення схеми моделювання.

Ключові слова: *молекулярна динаміка, водні суміші етанолу, поверхневий натяг, діелектрична проникність, парціальні молярні об'єми*